

Controlling Thin Film Surface Morphology for Improved Light Trapping

Jianqiao Huang, Xinyu Zhang, Gerassimos Orkoulas and Panagiotis D. Christofides

Abstract—This work demonstrates the use of feedback control, coupled with a suitable actuator design, in manufacturing thin films whose surface morphology is characterized by a desired visible light reflectance/transmittance level. The problem is particularly important in the context of thin film manufacturing for thin film solar cells where it is desirable to produce thin films with precisely tailored light trapping characteristics.

I. INTRODUCTION

Thin film solar cells constitute an important and growing component of the overall solar cell market (see, for example, [7], [17]) owing to their reduced cost relative to silicon-based solar cell modules as well as to the potential of using various thin film materials which may lead to improved light conversion efficiencies (currently on the order of 10% for production modules.) In addition to investigating the performance with respect to light conversion efficiency and long-term stability of an array of materials, thin film solar cell technology stands to benefit from optimal thin film manufacturing (deposition) control strategies that produce thin films with desired light reflectance and transmittance properties. Specifically, extensive research on optical properties of thin-film, primarily silicon, solar cells has demonstrated that the scattering properties of the thin film interfaces directly influence the light trapping ability and the efficiency of thin-film silicon solar cells (see, for example, [15], [14]). Shaping the morphology of the various surfaces and interfaces at the thin film deposition stage is therefore critical in order to maximize the amount of light trapped within the solar cell and converted to electrical energy. With respect to visible light trapping by thin film solar cells, the light scattering properties of the various surfaces/interfaces have a complex dependence on the surface morphology interface. While developing accurate models for predicting optical properties of thin films is an on-going research topic, it is well-established that the root-mean-square surface roughness and slope at characteristic length scales that are comparable to the wavelength of the visible light are key factors that influence thin film reflectance and transmittance (e.g.,

[4], [19]). Specifically, significant increase of conversion efficiency with appropriately roughened interfaces has been reported in several works [13], [12].

Over the last twenty years within the control engineering literature, extensive efforts have been made on the modeling and model-based feedback control of thin film deposition processes with emphasis on the problems of film thickness, roughness and porosity regulation. Microscopic modeling of thin film growth is usually carried out via kinetic Monte-Carlo (kMC) methods (see, for example, [6], [16], [3] for results and references in this area) as well as stochastic partial differential equations (e.g., [5], [20]). With respect to model-based feedback control of thin film deposition, early efforts focused on deposition spatial uniformity control on the basis of continuum-type distributed parameter models (e.g., [2]), while within the last ten years, most attention has focused on control of thin film surface morphology and microstructure. Since kMC models are not available in closed form and cannot be readily used for feedback control design and system-level analysis, stochastic differential equation (SDE) models (whose parameters are computed from kMC model data) have been used as the basis for the design of feedback controllers to regulate thin film surface roughness (e.g., [3], [18], [8]), film porosity and thickness [9]. In an attempt to manufacture thin film solar cells with optimal light conversion efficiencies, we recently initiated an effort towards modeling and control of thin film surface morphology to optimize thin film light reflectance and transmittance properties. To this end, we initially studied the dynamics and lattice size dependence of surface mean slope [10] and developed predictive control algorithms to regulate both surface roughness and slope at an atomic level using stochastic PDEs [22]. Taking advantage of these analysis and controller design results, we recently [23] made the first attempt to control thin film surface morphology at a length scale comparable to the visible light wavelength. Specifically, we addressed aspects of this problem with respect to predictive controller design using a stochastic PDE with a patterned deposition rate profile but we did not address the challenging problem of implementing the predictive controller on a large-lattice kinetic Monte-Carlo simulation that can cover a significant number of visible light wavelengths (which is on the order of 400nm – 700nm).

Motivated by the above considerations, this work presents an integrated control actuator and control algorithm design for the regulation of deposition of thin films such that the final thin film surface morphology is characterized by a desired visible light reflectance/transmittance level. To

Jianqiao Huang, Xinyu Zhang and Gerassimos Orkoulas are with the Department of Chemical and Biomolecular Engineering, University of California, Los Angeles, CA 90095-1592, USA. Panagiotis D. Christofides is with the Department of Chemical and Biomolecular Engineering and the Department of Electrical Engineering, University of California, Los Angeles, CA 90095-1592, USA. Emails: john841123@ucla.edu, xinyuzhang@ucla.edu, makis@seas.ucla.edu and pdc@seas.ucla.edu. P. D. Christofides is the corresponding author. Financial support from the National Science Foundation, CBET-0652131, and UCLA Doctoral Dissertation Year Fellowships for Xinyu Zhang and Jianqiao Huang are gratefully acknowledged.

demonstrate the approach, we focus on a thin film deposition process involving atom adsorption and surface migration and use a large-lattice (lattice size=40,000) kinetic Monte-Carlo simulation to describe its spatiotemporal behavior; this allows computing surface roughness and slope at different length-scales ranging from atomic scale to visible light wavelength scale. Subsequently, thin film surface morphology characteristics like roughness and slope are computed for different characteristic length scales and it is found that a patterned actuator design is needed to induce thin film surface roughness and slope at visible light wavelength spatial scales, that lead to desired thin film reflectance and transmittance values. An Edwards-Wilkinson-type equation is used to model the surface evolution at the visible light wavelength spatial scale and to form the basis for feedback controller design within a model predictive control framework. Simulation studies demonstrate that the proposed controller and patterned actuator design successfully regulate surface roughness and slope at visible light wavelength spatial scales to set-point values at the end of the deposition that yield desired levels of thin film reflectance and transmittance. An application to a large-scale kinetic Monte-Carlo model can be found in [11].

II. THIN FILM DEPOSITION PROCESS MODELING

In this section, a one-dimensional solid-on-solid (SOS) on-lattice kinetic Monte Carlo (kMC) model is used to simulate the thin film deposition process, which includes two microscopic processes: an adsorption process, in which particles are incorporated onto the film from the gas phase, and a migration process, in which surface particles move to adjacent sites. The width of the lattice is fixed so that the lattice contains a fixed number of sites in the lateral direction. The new particles are always deposited from the top side of the lattice with vertical incidence; see Fig.1. Particle deposition results in film growth in the direction normal to the lateral direction. The direction normal to the lateral direction is thus designated as the growth direction. The number of sites in the lateral direction is defined as the lattice size and is denoted by L . Periodic boundary conditions (PBCs) are applied at the edges of the lattice in the lateral direction. The top particles of each column are defined as the surface particles and the positions of the centers of all surface particles form the surface height profile. The number of nearest neighbors of a surface particle ranges from zero to two. A surface particle with zero nearest neighbors is possible to migrate to one of its adjacent columns with equal probability. A surface particle with one nearest neighbor is possible to migrate to its adjacent column with lower height with appropriate probability based on the migration rate (please see Eq. 1 below). A surface particle with two nearest neighbors can not migrate. Particles that are not on the film surface can not migrate.

In the adsorption process, a site is randomly selected with uniform probability among all lattice sites and a particle is deposited on top of this site. The overall adsorption rate, w , is expressed in the unit of layer per second. In the

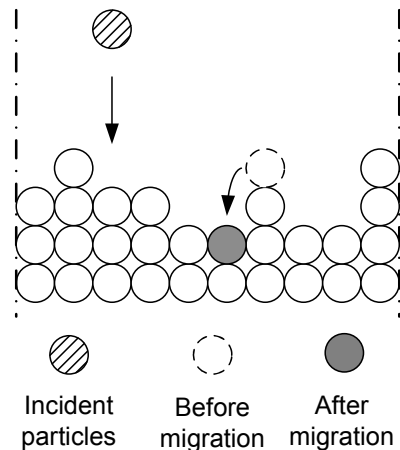


Fig. 1. Thin film growth process on a solid-on-solid one-dimensional square lattice.

migration process, a surface particle overcomes the energy barrier of the site and jumps to a vacant neighboring site. The migration rate (probability) of a particle follows an Arrhenius-type law with a pre-calculated activation energy barrier that depends on the local environment of the particle, i.e., the number of the nearest neighbors of the particle chosen for a migration event. The migration rate of the i th surface particle is calculated as follows:

$$r_m = v_0 \exp\left(-\frac{E_s + n_i E_n}{k_B T}\right) \quad (1)$$

where v_0 denotes the pre-exponential factor, n_i is the number of the nearest neighbors of the i th particle and can take the values of 0 and 1, (r_m is zero when $n_i = 2$ since in the one-dimensional lattice this surface particle is fully surrounded by other particles and cannot migrate), E_s is the contribution to the activation energy barrier from the site itself, E_n is the contribution to the activation energy barrier from each nearest neighbor, k_B is the Boltzmann's constant and T is the substrate temperature of the thin film. Since the film is thin, the temperature is assumed to be uniform throughout the film.

A. Surface morphology at atomic level

Thin film surface morphology, which can be expressed in terms of surface roughness and slope, is a very important surface property influencing the light trapping properties of thin films. Surface roughness is defined as the root-mean-square (RMS) of the surface height profile. Specifically, the definition of surface roughness is given as follows:

$$r = \left[\frac{1}{L} \sum_{i=1}^L (h_i - \bar{h})^2 \right]^{1/2} \quad (2)$$

where r denotes surface roughness, h_i , $i = 1, 2, \dots, L$, is the surface height at the i -th position in the unit of layer, L denotes the lattice size, and the surface mean height is given by $\bar{h} = \frac{1}{L} \sum_{i=1}^L h_i$.

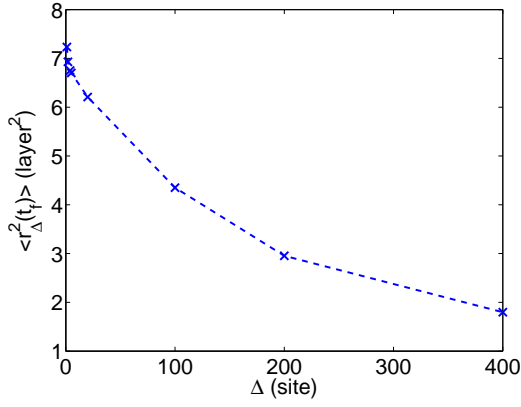


Fig. 2. Dependence of expected aggregate surface roughness on aggregation size obtained from kMC simulations; $t_f = 1000$ s.

In addition to surface roughness, another quantity that also determines the surface morphology is the surface mean slope. In this work, the surface mean slope is defined as the RMS of the surface gradient profile as follows:

$$m = \left[\frac{1}{L} \sum_{i=1}^L h_{s,i}^2 \right]^{1/2} \quad (3)$$

where m denotes the RMS slope and $h_{s,i}$ is the surface slope at the i -th lattice site, which is a dimensionless variable. The surface slope, $h_{s,i}$ is computed as follows:

$$h_{s,i} = \frac{h_{i+1} - h_i}{1} \quad (4)$$

Since the unit of height is layer and the distance between two adjacent particles (the diameter of particles) always equal to one layer, the denominator of $h_{s,i}$ is always one. Due to the use of PBCs, the slope at the boundary lattice site ($i = L$) is computed as the slope between the last lattice site (h_L) and the first lattice site (h_1).

To investigate the open-loop properties of surface morphology, a set of kMC simulations is carried out at different w with $T = 480$ K and $L = 40000$. In particular, the continuous-time Monte Carlo (CTMC) method is used in the kMC simulations. In this method, a list of events is constructed and an event is selected randomly with its respective probability. After the execution of the selected event, the list is updated based on the new lattice configuration. The following values are used for the parameters of the migration rate of Eq. 1, $\nu_0 = 10^{13} \text{s}^{-1}$, $E_s = 1.2$ eV and $E_n = 0$ eV.

B. Aggregate surface morphology and spatial deposition rate profile

One of the most important application of our work is to simulate and control the deposition process of thin film solar cells in order to improve solar cell efficiency via enhanced light trapping. However, the wavelength of visible light (400nm – 700nm) is much larger than the diameter of silicon atoms (~ 0.25 nm) and thus, it is necessary to define an aggregate surface morphology at length scales comparable to visible light wavelength.

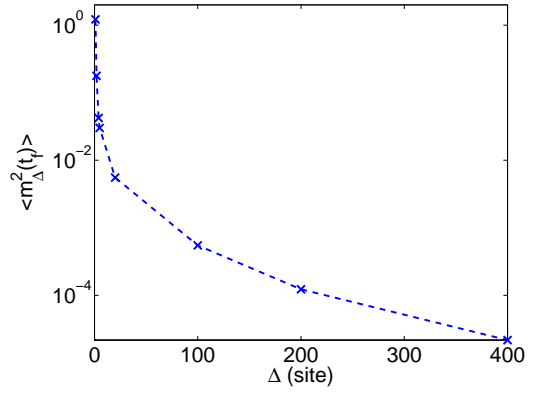


Fig. 3. Dependence of expected aggregate surface slope on aggregation size obtained from kMC simulations; $t_f = 1000$ s.

Specifically, the aggregate surface morphology is computed similarly to the atomic surface morphology, but on the basis of the aggregate surface height profile, $h_{\Delta,i}$, which is defined as follows:

$$h_{\Delta,i} = (h_{i\Delta+1} + h_{i\Delta+2} + \dots + h_{(i+1)\Delta}) / \Delta, i = 0, 1, \dots, L/\Delta - 1 \quad (5)$$

where $h_{\Delta,i}$ denotes the averaged surface height over the length scale of Δ sites, Δ denotes the aggregation size, i.e., the number of lattice sites used to calculate the aggregate surface height, and L/Δ denotes the number of aggregate sites of size Δ included in the spatial domain of the process. For the wavelength of visible light and silicon thin-film solar cells, the corresponding Δ is around 400; this follows from the fact that $0.25 \text{nm} \cdot 400 = 100 \text{nm}$, which is a length scale comparable to visible light wavelength. The definition of aggregate surface roughness and slope is given as follows:

$$r_{\Delta} = \left[\frac{1}{L} \sum_{i=1}^{L/\Delta} (h_{\Delta,i} - \bar{h}_{\Delta})^2 \right]^{1/2}, \quad (6)$$

$$m_{\Delta} = \left[\frac{1}{L} \sum_{i=1}^{L/\Delta} \left(\frac{h_{\Delta,i} - h_{\Delta,i+1}}{\Delta} \right)^2 \right]^{1/2}.$$

The dynamics of the aggregate surface roughness and slope are dependent on the characteristic length scale, Δ . To investigate this dependence, kMC simulations with $E_n = 0$ eV and $L = 40000$ were carried out. The expected aggregate surface roughness square, $\langle r_{\Delta}^2(t) \rangle$, and the expected aggregate surface slope square, $\langle m_{\Delta}^2(t) \rangle$, are calculated from the aggregate surface height profile from kMC simulations for different aggregation lengths. The simulation duration is $t_f = 1000$ s and 100 independent simulations were carried out to calculate the expected values of aggregate surface roughness and slope. Fig. 2 and Fig. 3 show the profiles of aggregate surface roughness square and slope square for different characteristic length scales, Δ . It is clear that the larger the characteristic length scale, the smaller the aggregate roughness and slope square. Furthermore, Fig. 3 shows that as the aggregation size increases, the aggregate slope square decreases very fast; a much weaker dependence

is observed for aggregate roughness in Fig. 2. From these results, we see that the corresponding aggregate slope square for $\Delta = 400$ is very small ($\langle m_{\Delta}^2 \rangle_{ss} \sim 10^{-5}$). This close-to-zero value of aggregate slope square reveals a smoothly changing surface profile with respect to characteristic length scales that are comparable to visible light wavelength. The smoothness of the surface profile persists at larger lattice sizes as well, due to the very weak lattice-size dependence of the mean slope square. This small aggregate slope square at large characteristic length scales is partly because the operating conditions are spatially uniform throughout the entire deposition process, i.e., the same deposition rate and substrate temperature are applied throughout the spatial domain. Thus, a spatially non-uniform deposition rate profile is necessary for the purpose of optimizing thin film light reflectance/transmittance by manipulation of film aggregate surface roughness and slope at length scales comparable to visible light wavelength; this conclusion is also consistent with recent experimental data [12]. To this end, we introduce a patterned in space deposition rate profile, which is defined as follows:

$$w(x) = w_0 + A \sin\left(\frac{2k\pi}{L}x\right), \quad A \leq w_0 \quad (7)$$

where x is a position along the lattice, w_0 is the mean deposition rate, A is the magnitude of the patterned deposition profile, k is the number of sine waves along the entire lattice, and L is the lattice size. Referring to the difference between w and w_0 , it is necessary to point out that w_0 is the mean deposition rate of the patterned deposition rate profile, $w(x)$, while the w used in subsection II-A is a spatially-uniform deposition rate.

The dynamics of aggregate surface morphology with patterned deposition rate profile is studied by carrying out a series of simulations at different mean deposition rates w_0 with $L = 40000$, $\Delta = 400$, $T = 480K$, $k = 5$ and $A = 0.1w_0$. The evolution profiles are shown in Fig. 4 and Fig. 5. The introduction of patterned deposition rate profiles significantly changes the dynamic profiles of aggregate surface morphology. Both aggregate roughness and aggregate slope can be increased by 10000 times by manipulating A compared to the aggregate surface morphology achieved with a uniform deposition rate profile. Thus, the introduction of a patterned deposition rate profile substantially expands the range of surface morphology values that can be obtained and makes light trapping optimization at length scales comparable to visible light wavelength possible.

III. CLOSED-FORM MODELING

A. Edward-Wilkinson equation of aggregate surface height

Given the complexity of the deposition process and the need to control surface roughness and slope at spatial scales comparable to the wavelength of visible light, the direct computation of a closed-form model, describing the surface height evolution and is suitable for controller design, from the microscopic deposition mechanisms is a very difficult (if not impossible) task. Therefore, a hybrid modeling approach

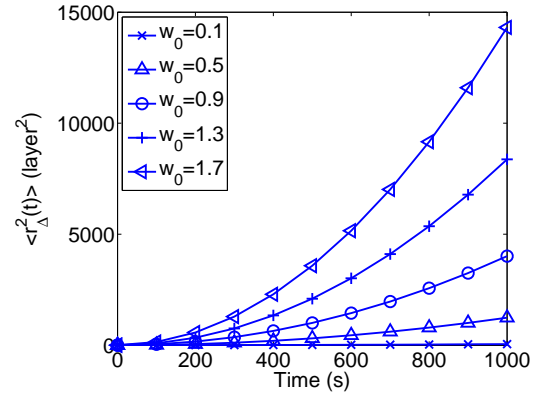


Fig. 4. Evolution of expected aggregate surface roughness with respect to time for different mean deposition rates (unit of w_0 is layer/s) obtained from kMC simulations. Patterned deposition with $k = 5$ and $A = 0.1w_0$.

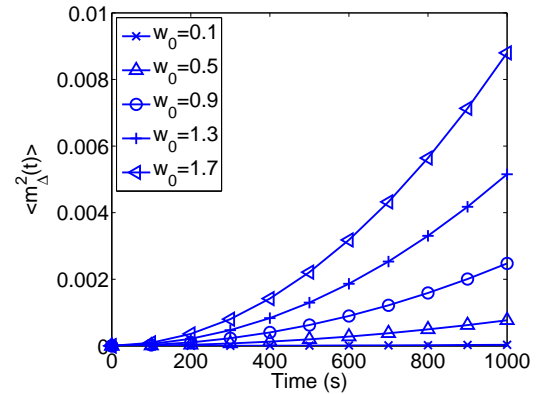


Fig. 5. Evolution of expected aggregate surface slope with respect to time for different mean deposition rates (unit of w_0 is layer/s) obtained from kMC simulations. Patterned deposition with $k = 5$ and $A = 0.1w_0$.

should be used in which a basic closed-form modeling structure is used and the model parameters are computed such that the predictions of key variables from the closed-form model are close (in a least-square sense) to the one of the kinetic Monte-Carlo model for a broad set of operating conditions. To this end, we use an Edward-Wilkinson(EW)-type equation, which is a second-order stochastic PDE to describe the aggregate surface height evolution and compute its parameters from kMC data. The choice of the EW-equation is motivated by the fact that it has been used in many deposition processes that involve a thermal balance between adsorption (deposition) and migration (diffusion) [1]. Specifically, a one-dimensional EW-type equation is used to describe the evolution of aggregate surface height profile:

$$\frac{\partial h_{\Delta}}{\partial t} = w(x,t) + c_2 \frac{\partial^2 h_{\Delta}}{\partial x^2} + \xi(x,t) \quad (8)$$

subject to the following periodic boundary conditions

$$h_{\Delta}(0,t) = h_{\Delta}(L,t), \quad \frac{\partial h_{\Delta}}{\partial x}(0,t) = \frac{\partial h_{\Delta}}{\partial x}(L,t) \quad (9)$$

and the initial condition $h_{\Delta}(x,0) = h_{\Delta}^0(x)$, where $x \in [0, L]$ is the spatial coordinate, t is the time, $h_{\Delta}(x,t)$ is the aggregate

surface height and $\xi(x, t)$ is a Gaussian white noise with zero mean and the following covariance:

$$\langle \xi(x, t) \xi(x', t') \rangle = \sigma^2 \delta(x - x') \delta(t - t') \quad (10)$$

where $\delta(\cdot)$ denotes the Dirac delta function. In Eq. 8, the parameters c_2 and σ^2 , corresponding to diffusion effects and stochastic noise respectively, depend on the deposition rate $w(x, t)$. In the case of a patterned deposition rate profile (control actuation), the term $w(x, t)$ is of the form:

$$w(x, t) = w_0(t) + A(t) \sin\left(\frac{2k\pi}{L}x\right) \quad (11)$$

where $w_0(t)$ is the mean deposition rate, $A(t)$ is the magnitude of patterned deposition rate, and k is the number of sine waves between 0 and L . Referring to the EW equation of Eq. 8, there are two model parameters, c_2 and σ^2 that must be determined as functions of the mean deposition rate w_0 and of the patterned deposition rate magnitude A . These parameters affect the dynamics of aggregate surface roughness and slope and can be estimated by fitting the predicted evolution profiles for aggregate surface roughness and slope from the EW equation to profiles of aggregate surface roughness and slope from kMC simulations. Least-square methods are used to estimate the model parameters, c_2 and σ^2 , so that the EW-model predictions are close in a least-square sense to the kMC simulation data. Based on c_2 and σ^2 values obtained from these fitting results, polynomial functions are chosen to estimate c_2 and σ^2 values at different w_0 with the least-square method. Specifically, a fourth order polynomial function with respect to w_0 is chosen to estimate c_2 and a linear function is chosen to estimate σ^2 , and the expressions are given as follows:

$$c_2(w) = a_{c_2}w^4 + b_{c_2}w^3 + c_{c_2}w^2 + d_{c_2}w + e_{c_2}, \quad (12)$$

$$\sigma^2 = a_{\sigma^2}w + b_{\sigma^2}$$

where a_{c_2} , b_{c_2} , c_{c_2} , d_{c_2} , e_{c_2} , a_{σ^2} and b_{σ^2} are time-invariant fitting model parameters. Due to space limitations, further details of the parameter estimation are omitted.

B. MPC formulation and simulations

We consider the problem of regulation of aggregate surface roughness and slope to desired levels within a model predictive control framework. Due to the stochastic nature of the variables, the expected values of aggregate surface roughness and slope, $\langle r_\Delta^2(t) \rangle$ and $\langle m_\Delta^2(t) \rangle$, are chosen as the control objectives. The mean deposition rate, w_0 , and magnitude of patterned deposition rate, A , are chosen as the manipulated inputs; the substrate temperature is fixed at $T = 480K$ during all closed-loop simulations. To account for a number of practical considerations, several constraints are added to the control problem. In particular, since $w(x) \geq 0$, the constraint $0 \leq A \leq w_0$ is imposed to ensure $w(x, t) > 0$, $\forall(x, t)$. To ensure the validity of the closed-form process model, there is a constraint on the range of variation of the mean deposition rate. Another constraint is imposed on the rate of change of the mean deposition rate to account for

actuator limitations. The control action at time t is obtained by solving a finite-horizon optimal control problem. The cost function in the optimal control problem includes penalty on the deviation of $\langle r_\Delta^2 \rangle$ and $\langle m_\Delta^2 \rangle$ from their respective set-point values. Different weighting factors are assigned to the aggregate surface roughness and slope. Aggregate surface roughness and slope have very different magnitudes, ($\langle r_\Delta^2 \rangle$ ranges from 10^2 to 10^4 and $\langle m_\Delta^2 \rangle$ ranges from 10^{-5} to 10^{-2}). Therefore, relative deviations are used in the formulation of the cost function to make the magnitude of the two terms comparable in the cost function. The optimization problem is subject to the dynamics of the aggregate surface height of Eq. 8. The optimal w_0 and A values are calculated at each sampling time by solving a finite-dimensional optimization problem in a receding horizon fashion. Specifically, the MPC problem at time t is formulated as follows:

$$\min_{w_0, A} \left(q_{r^2} \left[\frac{r_{set}^2 - \langle r_\Delta^2(t_f) \rangle}{r_{set}^2} \right]^2 + q_{m^2} \left[\frac{m_{set}^2 - \langle m_\Delta^2(t_f) \rangle}{m_{set}^2} \right]^2 \right) \quad (13)$$

where

$$\langle r_\Delta^2(t_f) \rangle = \frac{1}{L} \sum_{n=1}^{L/(2\Delta)} \sum_{p=1}^2 \langle z_{p,n}^2(t_f) \rangle, \quad (14)$$

$$\langle m_\Delta^2(t_f) \rangle = \sum_{n=1}^{L/(2\Delta)} \sum_{p=1}^2 (K_{p,n} \langle z_{p,n}^2(t_f) \rangle) \quad (15)$$

$$\langle z_{p,n}^2(t_f) \rangle = \text{var}(z_{p,n}(t_f)) + \langle z_{p,n}(t_f) \rangle^2 \quad (16)$$

$$\langle z_{p,n}(t_f) \rangle = e^{\lambda_n(t_f-t)} \langle z_{p,n}(t) \rangle + \frac{w_p}{\lambda_n} (e^{\lambda_n(t_f-t)} - 1) \quad (17)$$

$$\text{var}(z_{p,n}(t_f)) = e^{2\lambda_n(t_f-t)} \text{var}(z_{p,n}(t)) + \sigma^2(w) \frac{e^{2\lambda_n(t_f-t)} - 1}{2\lambda_n} \quad (18)$$

$$\lambda_n = -\frac{4c_2(w)\pi^2}{L^2}n^2 \quad (19)$$

subject to:

$$w_{min} \leq w_0 \leq w_{max}, \quad |w_0(t) - w_0(t-dt)| \leq \delta w_{max}, \quad (20)$$

$$w = w_0 + A \sin\left(\frac{k\pi x}{L}\right), \quad 0 \leq A \leq w_0 \quad (21)$$

and the fitting model of Eq.12, where t is the current time, dt is the sampling time, q_{r^2} and q_{m^2} are the weighting penalty factors for the deviations of $\langle r_\Delta^2 \rangle$ and $\langle m_\Delta^2 \rangle$ from their respective set-points at the i th prediction step, w_{min} and w_{max} are the lower and upper bounds on the mean deposition rate, respectively, and δw_{max} is the limit on the rate of change of the mean deposition rate. The optimal control actions are obtained from the solution of the multivariable optimization problem of Eq. 13, and are applied to the deposition process model over dt (i.e., either the EW equation model or the kMC model) during the time interval $(t, t + dt)$. At time $t + dt$, a new measurement of aggregate surface roughness and slope is received by the controller and the MPC problem of Eq. 13 is solved for the next set of control actions. An

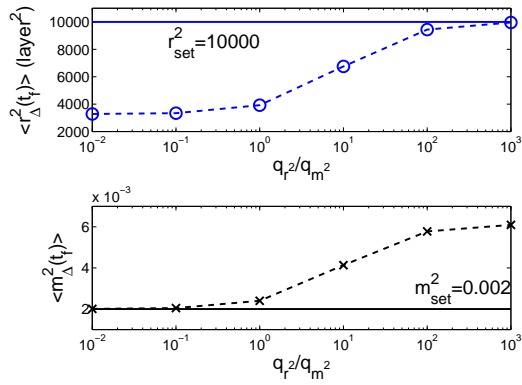


Fig. 6. $\langle r_{\Delta}^2(t_f) \rangle$ and $\langle m_{\Delta}^2(t_f) \rangle$ at the end of closed-loop simulations ($t = 100$ s) for different penalty weighting factors in the predictive controller with kMC model as the plant model. $10^{-2} \leq q_{r2} \leq 10^3$, $q_{m2} = 1$, $r_{set}^2 = 10000$ and $m_{set}^2 = 0.002$.

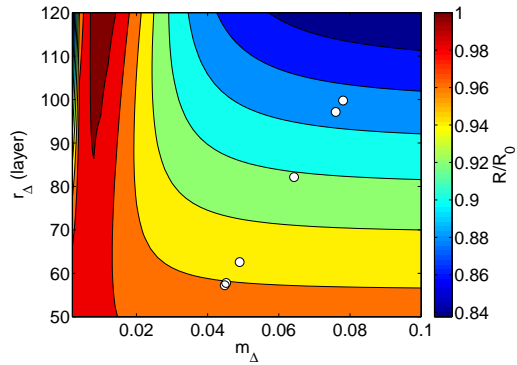


Fig. 7. Light reflectance of thin films deposited under closed-loop operations with different weighting factor ratios. $q_{r2} = 10^{-2}, 10^{-1}, 10^0, 10^1, 10^2$ and 10^3 (corresponding to small circles inside the figure from left to right), $q_{m2} = 1$, $r_{set}^2 = 10000$ and $m_{set}^2 = 0.002$.

interior point method optimizer, IPOPT [21], is used to solve the optimization problem in the MPC formulation.

Simultaneous regulation of aggregate surface roughness and slope has been investigated. The weighting factor of aggregate slope square, q_{m2} , is kept at 1, and the weighting factor of aggregate roughness square, q_{r2} , ranges from 10^{-2} to 10^3 . Fig. 6 shows the values of expected aggregate roughness and slope at the end of simulations as a function of q_{r2}/q_{m2} . It can be seen that the expected value of aggregate roughness approaches its set-point as q_{r2} increases at the cost of larger deviation of the aggregate slope from its set-point. Finally, we demonstrate an application of the proposed modeling and control framework to improve thin film solar cell performance. Fig. 7 shows how films with different reflectance values can be produced by simultaneous regulation of film surface aggregate roughness and aggregate slope. Specifically, the weighting factor of aggregate slope square, q_{m2} , is kept at 1, and the weighting factor of aggregate roughness square, q_{r2} , ranges from 10^{-2} to 10^3 , and the resulting aggregate roughness and slope are used to compute the light reflectance of the thin film according to [4]. It is clear that films with different reflectance values can be generated by regulating aggregate surface roughness and slope; please see the small circles in Fig. 7.

REFERENCES

- [1] C. Buzea and K. Robbie. State of the art in thin film thickness and deposition rate monitoring sensors. *Reports on Progress in Physics*, 68:385–409, 2005.
- [2] P. D. Christofides. *Nonlinear and Robust Control of PDE Systems: Methods and Applications to Transport-Reaction Processes*. Birkhäuser, Boston, 2001.
- [3] P. D. Christofides, A. Armaou, Y. Lou, and A. Varshney. *Control and Optimization of Multiscale Process Systems*. Birkhäuser, Boston, 2008.
- [4] H. Davies. The reflection of electromagnetic waves from a rough surface. *Proceedings of the IEE-Part IV: Institution Monographs*, 101:209–214, 1954.
- [5] S. F. Edwards and D. R. Wilkinson. The surface statistics of a granular aggregate. *Proceedings of the Royal Society of London Series A - Mathematical Physical and Engineering Sciences*, 381:17–31, 1982.
- [6] D. T. Gillespie. A general method for numerically simulating the stochastic time evolution of coupled chemical reactions. *Journal of Computational Physics*, 22:403–434, 1976.
- [7] M. A. Green. Thin-film solar cells: Review of materials, technologies and commercial status. *Journal of Materials Science: Materials in Electronics*, 18:15–19, 2007.
- [8] G. Hu, J. Huang, G. Orkoulas, and P. D. Christofides. Investigation of film surface roughness and porosity dependence on lattice size in a porous thin film deposition process. *Physical Review E*, 80:041122, 2009.
- [9] G. Hu, G. Orkoulas, and P. D. Christofides. Regulation of film thickness, surface roughness and porosity in thin film growth using deposition rate. *Chemical Engineering Science*, 48:3903–3913, 2009.
- [10] J. Huang, G. Hu, G. Orkoulas, and P.D. Christofides. Dynamics and lattice-size dependence of surface mean slope in thin-film deposition. *Ind. & Eng. Chem. Res.*, 50:1219–1230, 2010.
- [11] J. Huang, X. Zhang, G. Orkoulas, and P. D. Christofides. Dynamics and control of aggregate thin film surface morphology for improved light trapping: Implementation on a large-lattice kinetic Monte-Carlo model. *Chemical Engineering Science*, 66:5955–5967, 2011.
- [12] O. Isabella, J. Krč, and M. Zeman. Modulated surface textures for enhanced light trapping in thin-film silicon solar cells. *Applied Physics Letters*, 97:101106, 2010.
- [13] J. Krč and M. Zeman. Experimental investigation and modelling of light scattering in a-si:h solar cells deposited on glass/zno:al substrates. *Material Research Society Proceedings*, 715, 2002.
- [14] J. Muller and B. Rech. TCO and light trapping in silicon thin film solar cells. *Solar Energy*, 77:917–930, 2004.
- [15] A. Poruba, A. Fejfar, Z. Remeš, J. Špringer, M. Vaněček, and J. Kočka. Optical absorption and light scattering in microcrystalline silicon thin films and solar cells. *Journal of Applied Physics*, 88:148–160, 2000.
- [16] J. S. Reese, S. Raimondeau, and D. G. Vlachos. Monte Carlo algorithms for complex surface reaction mechanisms: Efficiency and accuracy. *Journal of Computational Physics*, 173:302–321, 2001.
- [17] W. van Sark, G. W. Brandsen, M. Fleuster, and M. P. Hekkert. Analysis of the silicon market: Will thin films profit? *Energy Policy*, 35:3221–3125, 2007.
- [18] A. Varshney and A. Armaou. Optimal operation of GaN thin-film epitaxy employing control vector parametrization. *AIChE Journal*, 52:1378–1391, 2006.
- [19] T.V. Vorburger, E. Marx, and T.R. Lettieri. Regimes of surface-roughness measurable with light-scattering. *Applied Optics*, 32:3401–3408, 1993.
- [20] D. D. Vvedensky, A. Zangwill, C. N. Luse, and M. R. Wilby. Stochastic equations of motion for epitaxial growth. *Physical Review E*, 48:852–862, 1993.
- [21] A. Wächter and L.T. Biegler. On The Implementation of an Interior-point Filter Line-search Algorithm for Large-scale Nonlinear Programming. *Mathematical Programming*, 106(1):25–57, 2006.
- [22] X. Zhang, G. Hu, G. Orkoulas, and P.D. Christofides. Multivariable model predictive control of thin film surface roughness and slope for light trapping optimization. *Ind. & Eng. Chem. Res.*, 49:10510–10516, 2010.
- [23] X. Zhang, J. Huang, G. Orkoulas, and P.D. Christofides. Controlling aggregate thin film surface morphology for improved light trapping using a patterned deposition rate profile. *Chemical Engineering Science*, 67:101–110, 2012.